Journal of Membrane Science 727 (2025) 124090

Contents lists available at ScienceDirect

Journal of Membrane Science

journal homepage: www.elsevier.com/locate/memsci

Deep eutectic solvent- and nanocellulose-tuned MXene membranes for efficient gas separation

Mengjie Li [1], Chuan Xu [1], Miaomiao Wu, Xiong-Fei Zhang [*], Jianfeng Yao [**]

Jiangsu Co-Innovation Center of Efficient Processing and Utilization of Forest Resources, College of Chemical Engineering, Nanjing Forestry University, Nanjing 210037, China

ARTICLE INFO

Keywords:
Deep eutectic solvent
Nanocellulose
Gas separation
MXene
Membrane

ABSTRACT

MXene-based membranes exhibit significant potential for gas separation. However, two major challenges persist: regulating the interlayer spacing of 2D MXenes and mitigating non-selective voids within the membrane structure. In this work, composite membranes comprising cellulose nanocrystals (CNCs), MXenes, and choline chloride/urea deep eutectic solvent (DES) were fabricated, and they contained carbon dioxide (CO_2)-selective nanochannels. The incorporation of DES effectively modulates the interlayer spacing of MXene nanosheets to match CO_2 molecules. Moreover, CNCs act as a continuous polymer skeleton, forming hydrogen bonds with adjacent MXenes to increase the inorganic–organic interface affinity. This design facilitates CO_2 transport through multiple mechanisms: (i) the solution-diffusion properties of the CNC-based polymer phase; (ii) optimized 2D MXene channels with an appropriate interlayer spacing to accelerate CO_2 permeation; and (iii) the amine groups in the alkaline DES as CO_2 carriers. The membrane demonstrated exceptional gas separation capabilities, attaining a maximum CO_2 permeability of 496.7 Barrer, along with ideal selectivities for CO_2/N_2 and CO_2/CH_4 of 78.8 and 90.3, respectively. This research proposes a novel strategy for regulating the interlayer spacing of MXenes and designing nanocellulose-based separation membranes.

1. Introduction

Carbon dioxide (CO_2) emitted from the combustion of fossil fuels is widely acknowledged as a key contributor to global warming and climate change [1,2]. In recent years, membrane-based technology for CO_2 separation has gained prominence as a highly energy-efficient and economically viable alternative to traditional methods, such as cryogenic distillation and solvent absorption [3,4]. A diverse range of inorganic and polymeric materials have been investigated as potential membrane candidates for gas separation [5,6]. Despite the high CO_2 separation performance achieved by membranes reported in the literature, the intrinsic trade-off between permeability and selectivity remains a significant hurdle, limiting the practical deployment of gas separation membranes [7,8]. Among the various materials explored, 2D materials have been extensively applied in gas separation processes, with MXene materials attracting particular attention and demonstrating immense potential [9–11].

MXenes, with the general formula of $M_{n+1}X_nT_X$, are fabricated by selectively etching the A-group layers from the $M_{n+1}AX_n$ phases [12,13]. They feature abundant surface-terminating groups (such as = O, –OH, and –F) that are uniformly distributed across the nanosheets, creating narrow channels between stacked MXene layers [14]. The gas permeability of MXenes is related to their interlayer spacing, wherein optimal channel dimensions facilitate the rapid transport of CO_2 through the membrane by establishing a preferential permeation pathway [15]. To precisely regulate the delamination behavior of MXene nanosheets, diverse CO_2-facilitated agents, including metal ions, amine agents, metal salts, ionic liquids, and deep eutectic solvents (DESs), have been explored [16]. Among these, DESs have garnered significant attention owing to their facile synthesis process, cost-effectiveness, nontoxic nature and good CO_2 capture capability [17].

DESs are a class of binary or ternary eutectic mixtures comprising hydrogen bond donors and hydrogen bond acceptors [18,19]. Lin et al. intercalated a choline chloride/ethylene glycol (ChCl/EG) DES into MXene nanosheets to prepare CO_2 separation membranes [17]. Leveraging the CO_2 affinity and solubility of DESs, the composite

* Corresponding author.
** Corresponding author.
E-mail addresses: zxf1990@njfu.edu.cn (X.-F. Zhang), jfyao@njfu.edu.cn (J. Yao).
[1] These authors contributed equally to this work.

https://doi.org/10.1016/j.memsci.2025.124090
Received 4 February 2025; Received in revised form 5 April 2025; Accepted 8 April 2025
Available online 8 April 2025

membranes exhibited a CO_2 permeance of 26.4 GPU, with ideal selectivities over N_2, CH_4, and H_2 of 319.1, 249.0, and 12.4, respectively. Prior studies have focused mainly on the development of ultrathin MXene membranes with CO_2-selective channels [20]. Although high gas flux can be obtained, it is challenging to prepare defect-free MXene--based membranes, primarily because of the mechanical brittleness of MXenes [14]. One effective strategy is integrating MXenes into a polymer matrix [21]. For example, Yahia et al. confined MXene nanosheets into a PIM-1 matrix, and the results demonstrated that the introduction of MXenes effectively increased gas solubility and diffusivity [22]. The optimal sample achieved a low CO_2/CH_4 separation selectivity of 13.5, accompanied by a CO_2 permeability of 7652 Barrer. Overall, breaking the selectivity−permeability limit and enhancing the affinity of the MXene/polymer interface are difficult.

In our previous work, we demonstrated that nanocellulose is a good polymer matrix for gas separation membrane fabrication because of its exceptional solubility−selectivity characteristics and ease of processing [23,24]. The abundant carboxyl/hydroxyl groups located on the nanocellulose surface provide negative charge points and anchor sites for the attachment of inorganic fillers, contributing to good interface affinity [25]. Here, a ternary DES/MXene/nanocellulose membrane is designed. An alkaline ChCl/urea DES with sufficient amine groups was synthesized and used to intercalate the MXene nanosheets. This DES system can combine CO_2-carrier functionality with the tuning ability of the MXene interlayer [26]. In addition, the polymer phase of CNCs can form hydrogen bonds with adjacent MXenes and optimize the interlayer spacing of MXenes [27]. CO_2 transport is accelerated by combining the solution-diffusion properties of the CNCs and designing MXene channels with suitable interlayer spacings and amine groups in the DES. The composite membranes were evaluated via single and mixed gas separation to evaluate their CO_2 separation capability.

2. Experimental

2.1. Materials

Choline chloride (ChCl, 99.0 %) and hydrochloric acid (HCl, AR) were purchased from Nanjing Chemical Reagent Company. Urea was obtained from Sinopharm Chemical Reagent Company (AR). Cellulose nanocrystal (CNC) powder (length ca. 200 nm, diameter ca. 10 nm) and lithium fluoride (LiF, AR) were obtained from Shanghai McLean Biochemical Technology Company. Titanium aluminum carbide (Ti_3AlC_2, 98 %) was purchased from Rhawn Chemical Reagent Company. The nylon substrate, with a diameter of 50 mm and a pore size of 200 nm, was procured from Tianjin Jinteng Experimental Equipment Company. CO_2, N_2, and CH_4 with purities ≥99.99 % were purchased from Nanjing Special Gas Factory Company.

2.2. Synthesis of ChCl/urea DES

For DES synthesis, ChCl and urea were dried separately at 80 °C under vacuum for 1 h. Then, the ChCl and urea were mixed at a 1:2 M ratio in a sealed bottle. The mixture was stirred at 60 °C for 2 h until a transparent, homogeneous liquid was obtained.

2.3. Synthesis of $Ti_3C_2T_x$ nanosheets

The synthesis method of $Ti_3C_2T_x$ nanosheets was modified from previous literature [28]. Briefly, $Ti_3C_2T_x$ nanosheets were synthesized by selectively etching Al from Ti_3AlC_2 via HF. Specifically, 1 g of LiF and 1 g of Ti_3AlC_2 were added to 20 mL of HCl (9 mol L^{-1}) in a PTFE beaker. The mixture was continuously stirred at 50 °C (550 rpm) for 72 h. The mixture was subsequently washed with deionized water (DI) until the pH reached 7. The resulting black solid residue, which was $Ti_3C_2T_x$ MXene, was then sonicated for 1 h and centrifuged to collect the delaminated MXene nanosheets. Afterward, the collected solids were freeze-dried in a Petri dish for 12 h at −65 °C under vacuum to yield the water-intercalated $Ti_3C_2T_x$ MXene powder (denoted as Water-I MXene).

2.4. Intercalation and delamination of $Ti_3C_2T_x$ with DES

0.1 g of as-prepared water-intercalated $Ti_3C_2T_x$ nanosheets was added to the ChCl/urea DES (5 mg mL^{-1}, 20 mL). The mixture was sonicated in an ice–water bath for 1 h, followed by stirring for 1 week. Next, the mixture was vacuum-filtered through a nylon membrane and washed with DI water and ethanol (200 mL). After freeze-drying in a Petri dish for 12 h at −65 °C under vacuum, the DES-intercalated MXene powder was obtained (denoted as DES-I MXene).

2.5. Assembly of composite membranes

For the composite membrane preparation, 5, 10, 15, 20, and 25 mg of the as-prepared DES-I MXene powder was added to 5 mL of DES solution to obtain a DES/MXene suspension at concentrations of 1, 2, 3, 4, and 5 mg mL^{-1}. Then, 5 mg of CNC powder was added to 5 mL of DES solution to obtain a DES/CNC dispersion at a concentration of 1 mg mL^{-1}. The suspension was stirred separately at room temperature (550 rpm) for 6 h. Subsequently, 5 mL of DES/MXene suspension and 5 mL of DES/CNC suspension were mixed, sonicated for 30 min, and stirred for an additional 6 h. Finally, the mixture was vacuum-filtered on the porous nylon substrate for 5 h and placed in a constant temperature and humidity chamber (relative humidity of 40 %, temperature of 35 °C) for 24 h to obtain the ternary membrane. The resulting membranes were labeled DES/MXene/CNC-X, where X (=1, 2, 3, 4, 5) corresponds to the concentration of MXene in the DES/MXene suspension (1, 2, 3, 4, or 5 mg mL^{-1}). For comparison, a hybrid MXene/CNC membrane consisting of water-intercalated MXene powder and CNCs was also prepared under similar conditions, where 20 mg of as-prepared Water-I MXene powder was used, and all the DES solution was replaced with DI water.

2.6. Characterizations

The membrane materials were characterized via X-ray diffraction (XRD), scanning electron microscopy (SEM), energy-dispersive X-ray spectroscopy (EDX), transmission electron microscopy (TEM), atomic force microscopy (AFM), N_2 adsorption−desorption, Fourier transform infrared spectroscopy (FT-IR) and thermogravimetric analysis (TGA). Detailed information on the characterization techniques is provided in the Supporting Information. Single-gas and mixed-gas separation experiments were conducted using a custom-made apparatus (Scheme S1).

3. Results and discussion

3.1. Characterization of DES-intercalated MXenes

In this work, MXene nanosheets were synthesized by selectively etching Al from Ti_3AlC_2. Afterward, a designed ChCl/urea DES was used as an intercalating agent to intercalate the MXene layers. A schematic illustration of the interaction between DESs and MXenes is displayed in Fig. 1a. The DES solvent adheres to the surface of the MXene, forming strong hydrogen bonds with the surface-terminating groups of the MXene [29]. Therefore, the interlayer spacing of MXenes is regulated by the newly formed cross-links. For comparison, DI water was used as an intercalating agent to tune the MXene nanosheets.

XRD was conducted to analyze the crystal structure of the MXene nanosheets intercalated with water and DES (Fig. 1b). The diffraction pattern of the water-treated sample presents a distinct peak at 6.62°, which corresponds to the (002) plane. The interlayer spacing calculated from Bragg's law is approximately 1.34 nm, which is typical of multilayer MXenes [20]. In contrast, in the DES-treated sample, the characteristic peak of the (002) plane shifts to a lower angle of 6.16°, indicating an increase in the interlayer spacing to approximately 1.43 nm. This

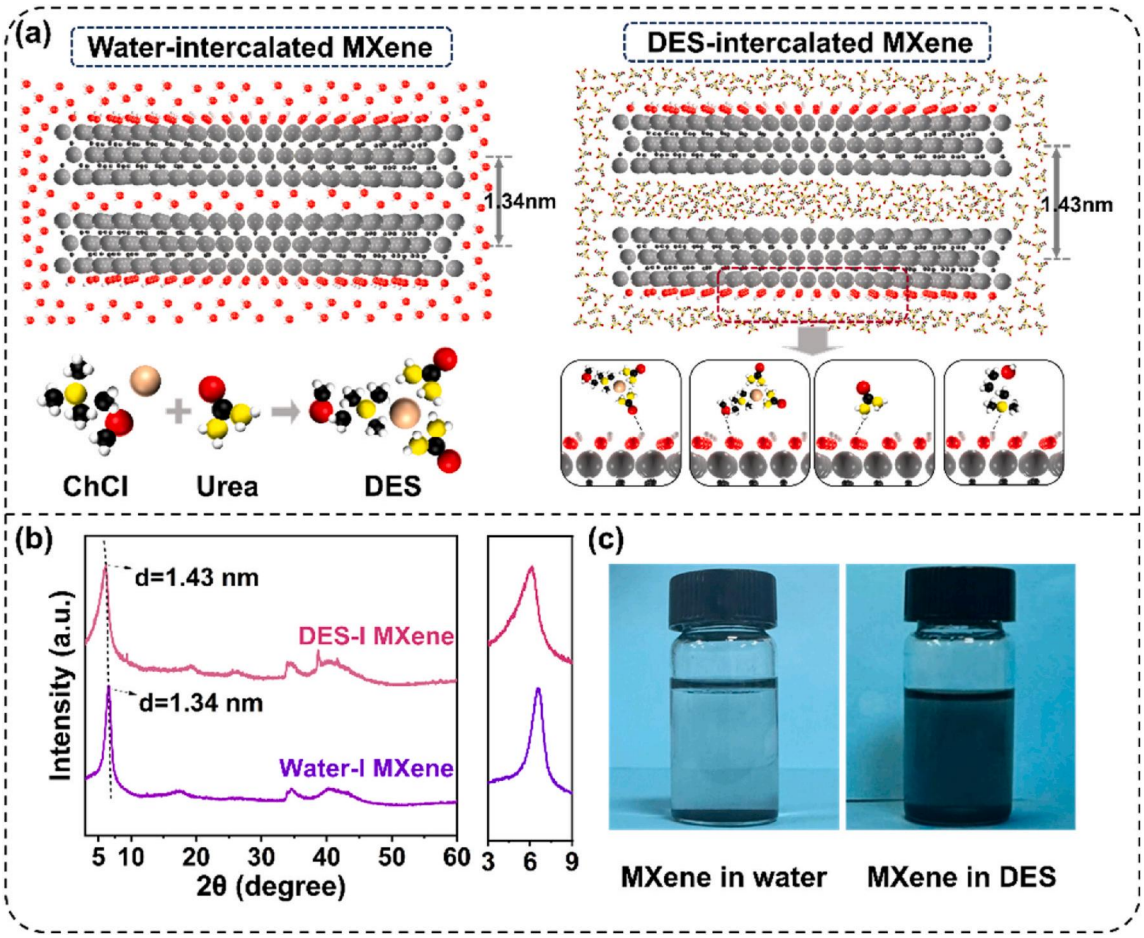

Fig. 1. (a) Schematic illustration of the intercalation of water and ChCl/urea DES into MXene nanosheets. (b) XRD patterns of the MXene nanosheets intercalated with water and ChCl/urea DES. (c) Dispersion of MXene in water and in DES for 1 week.

result suggests that the spontaneous intercalation of DES molecules leads to an expansion of the interlayer spacing. The dispersion stability of MXenes in DESs over a long period of time is significantly better than that in water (Fig. 1c and Fig. S1). In addition, DESs can reduce the MXene thickness by decreasing the number of stacked layers [30,31].

The morphology of the multi-layer MXene nanosheets after intercalation was examined *via* SEM. After etching Al from pristine Ti_3AlC_2, the MXene exhibits an accordion-like layered structure (Fig. S2a). When the MXene nanosheets were treated with water, there was no obvious morphology change (Fig. 2a). The introduction of DES promotes the delamination of MXenes (Fig. 2b). TEM images reveal that the intercalation of DES leads to a reduction in the lateral size and a decrease in the thickness of the delaminated layers (Fig. 2c and d). This was due to the combined effect of ultrasonic treatment and DES addition, which appeared to exfoliate the multilayer MXene into smaller nanosheets [32]. After DES treatment, the ultrathin MXene nanosheets appear nearly transparent under the electron beam. To further confirm the morphology and size changes of the MXenes, atomic force microscopy (AFM) images of the water- and DES-intercalated MXene nanosheets are shown in Fig. 2e and f. Upon water intercalation, the MXene nanosheets display a lateral size of approximately 1–2 μm and an average thickness of 3.8 nm. The DES-treated MXene nanosheets have a reduced lateral size of 300 nm and an average thickness of 2.9 nm. N_2 adsorption–desorption isotherms reveal that the specific surface areas of the water-treated and DES-treated samples were 2.3 and 7.3 $m^2\ g^{-1}$, respectively (Fig. S2b). The presence of DES reduces the lateral size and enlarges the interlayer spacing, leading to an increase in surface area. The increased surface area and optimized MXene nanochannels are expected to accelerate CO_2 adsorption and permeation.

3.2. *Characterization of the composite membranes*

The DES-I MXene nanosheets exist in powder form and are used as fillers. Fig. 3a illustrates the fabrication process of the DES/MXene/CNC membrane (more details are provided in Fig. S3). For comparison, Water-I MXene was integrated into the CNC matrix to obtain hybrid MXene/CNC membranes. The CNC has a rod-like structure, with a diameter of ca. 10 nm and a length of ca. 200 nm. The introduction of CNCs has two roles: (i) serving as a continuous phase in the membrane structure and (ii) stabilizing the interlayer spacing of the MXene nanosheets. Unlike DESs, it is difficult for CNCs to enter the interlayer nanochannels of MXenes. However, the abundant surface hydroxyl groups on the CNC surface can construct hydrogen bonds with the DES, thus regulating and balancing the distance between adjacent MXene nanosheets [33].

To better understand the interactions within the composite membrane, the functional groups were analyzed via FT-IR. As shown in Fig. 3b, the peak at 960 cm^{-1} is attributed to the asymmetric C–C–O stretching vibration of the choline cation group [34]. The characteristic band at 2970 cm^{-1} is assigned to the C–H stretching vibration of the cellulose backbone [35]. The peak at 1094 cm^{-1} is attributed to the C–N asymmetric stretching vibration, confirming the successful introduction of DES [17]. The distinctive peak observed at 3450 cm^{-1} is associated with the stretching vibration of –OH. This phenomenon is related to the hydrogen bonds within the membrane. The increased –OH stretching intensity with increasing DES content reflects increased hydrogen

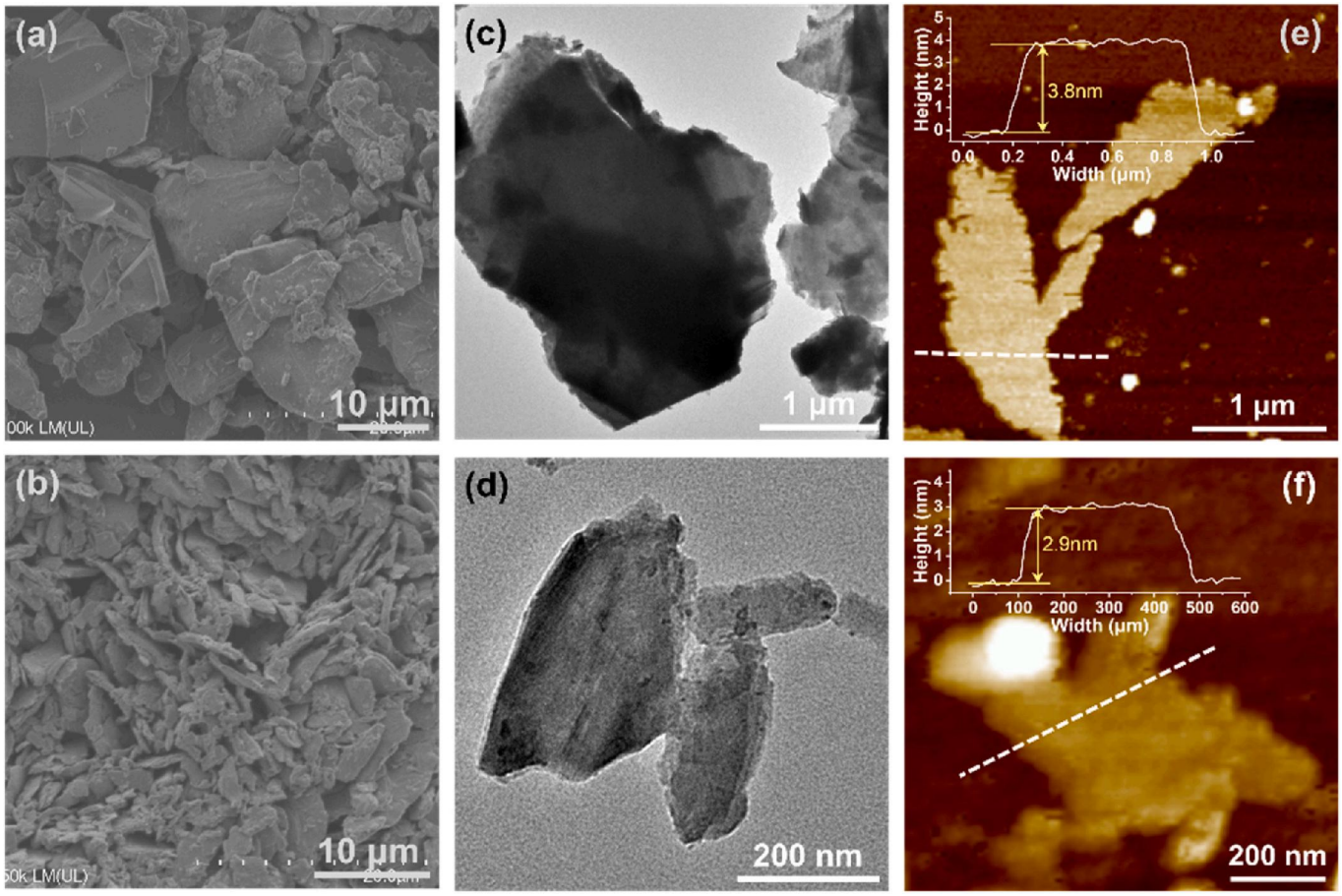

Fig. 2. SEM, TEM and AFM images of (a, c, e) Water-I MXene nanosheets and (b, d, f) DES-I MXene nanosheets.

bonding density through peak broadening and a redshift [36]. The absorption peaks observed in the FT-IR spectrum within the range of 3700-3000 cm^{-1} were subjected to further analysis to investigate the alterations in hydrogen bonding (Fig. 3c and d). The intermolecular hydrogen bonds O(6)H··· O(3) and intramolecular hydrogen bonds O(3)H··· O(5) and O(2)H···O(6) were distinguished. Moreover, intermolecular hydrogen bonding is significantly strengthened after the introduction of DES-I MXene because of the establishment of new hydrogen bonds with cellulose [36,37]. TGA was conducted to assess the thermal stability of the MXene and the composite membranes (Fig. 3e). The curve of the MXene indicates a weak weight loss, demonstrating the good thermal stability of the MXene. Except for the MXene samples, the TGA curves of the other samples exhibit two-step weight loss. The weight loss observed below 100 °C is indicative of moisture desorption, and the second stage at around 250 °C is associated with the decomposition of cellulose and DES components [24].

The appearance of DES/MXene/CNC-4 reveals a smooth and glossy surface (Fig. S4). The micro-morphology of the membranes was observed via SEM. Fig. 4a, c show the top and cross-sectional surface morphology of the MXene/CNC membrane. It presents a relatively rough surface, with a thickness of about 7.2 μm. Upon the addition of DES, the DES/MXene/CNC-4 membrane has a smooth surface without noticeable defects (Fig. 4b), with a thickness of about 9.8 μm. Moreover, the DES facilitates the orderly stacking of the MXene nanosheets and CNCs, as the DES/MXene/CNC-4 membrane possesses a densely packed layered structure (Fig. 4d and Fig. S5). This suggests that the hydrogen bonding network induces laminated stacking of MXenes and CNCs during membrane assembly [38]. DES-induced layer alignment reduces tortuosity, offsetting any path-length increase from spacing expansion. The corresponding EDX mapping images of F, Ti, and N elements prove the uniform distribution of MXene and DES throughout the membrane matrix (Fig. 4e).

The change in the interlayer spacing can be verified by the XRD results. The interlayer spacing of the composite membrane was analyzed via XRD (Fig. 4f). The diffraction pattern of the MXene/CNC membrane exhibits a peak at 6.34°, corresponding to an interlayer spacing of 1.39 nm. After DES modification, the peak shifts to 6.06°, indicating an increase in the interlayer spacing to 1.46 nm. Compared with the water-intercalated MXene nanosheets (1.34 nm), the MXene/CNC membrane has a 0.05 nm greater interlayer spacing. Compared with that of the DES-treated MXene nanosheets (1.43 nm), the interlayer spacing of the DES/MXene/CNC membrane increases by 0.03 nm. It can be concluded that cellulose also influences the interlayer spacing [39]. In addition, the content of DES-I MXene has a negligible effect on the interlayer spacing.

3.3. Gas separation performance

The efficacy of the membranes in gas separation was evaluated via a specially designed gas separation apparatus. The tests were conducted at a steady state under ambient conditions (25 °C and 0.1 MPa). For all the membranes, the tested gas permeabilities followed the order of CO_2 (0.33 nm), N_2 (0.36 nm), and CH_4 (0.38 nm). As shown in Fig. 5a, the MXene/CNC membrane exhibits a maximum permeability of 50.0 Barrer, accompanied by ideal selectivities for CO_2/N_2 and CO_2/CH_4 of 10 and 12.5, respectively. The introduction of DES increases both the CO_2 permeability and gas selectivity. This improvement is attributed to the optimized interlayer spacing of the MXene nanosheets, which creates rapid transport channels favorable for CO_2. The DES plays a decisive role in interlayer spacing regulation, making the DES/MXene/CNC membranes optimal for selective CO_2 sieving. In addition, the amine groups

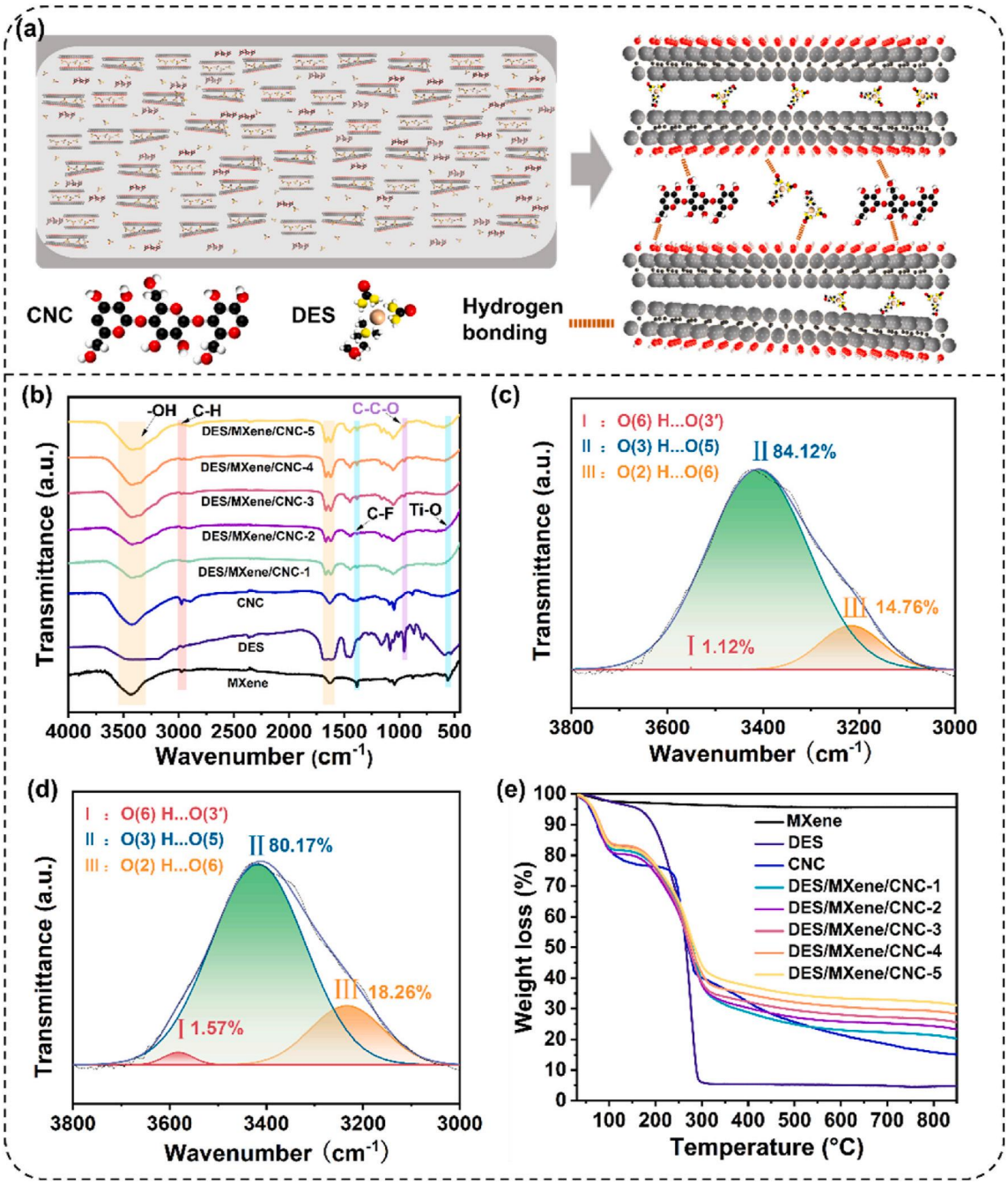

Fig. 3. (a) Schematic illustration of the preparation process of the DES/MXene/CNC membrane. (b) FT-IR spectra of the MXene nanosheets, DES, CNC and composite membranes. H-bond models of (c) CNCs and (d) DES/MXene/CNC-4 obtained from FT-IR in the range of 3700-3000 cm^{-1}. (e) TGA curves of MXene nanosheets, DES, CNC and composite membranes.

in the alkaline DES can act as CO_2 carriers and accelerate CO_2 permeation [40].

The effects of DES-I MXene loading on gas separation performance were investigated. As the DES-I MXene content increased, the CO_2 permeability gradually decreased, whereas the gas selectivity significantly improved. The best performance was observed for DES/MXene/CNC-4, with a CO_2 permeability of 496.7 Barrer and CO_2/N_2 and CO_2/CH_4 ideal selectivities of 78.8 and 90.3, respectively. This result suggests that an increase in the DES-I MXene content creates more CO_2-selective pathways within the membrane. However, this also slightly increases the mass transfer resistance, affecting CO_2 permeability. When the DES-I MXene content increased further in the DES/MXene/CNC-5 membrane, both the CO_2 permeability and gas selectivity decreased sharply, possibly due to the formation of non-selective channels between MXene nanolayers. When the MXene content is too high, it will cause the nanosheets to stack irregularly and increase the tortuosity of the gas transport pathways, leading to increased mass transfer resistance.

The effect of feed pressure on the separation performance of DES/MXene/CNC-4 was studied across a transmembrane pressure range of 0.1–0.5 MPa. As shown in Fig. 5b, the CO_2 permeability decreases from 510.7 Barrer to 485.7 Barrer with increasing pressure. At higher pressures, the available CO_2 adsorption sites become occupied, reducing the driving force for CO_2 transport. However, the N_2 and CH_4 permeabilities remain relatively stable with minimal fluctuations. This suggests that the interlayer spacing remains stable despite changes in pressure, ensuring consistent gas transport within the membrane. A 360-h

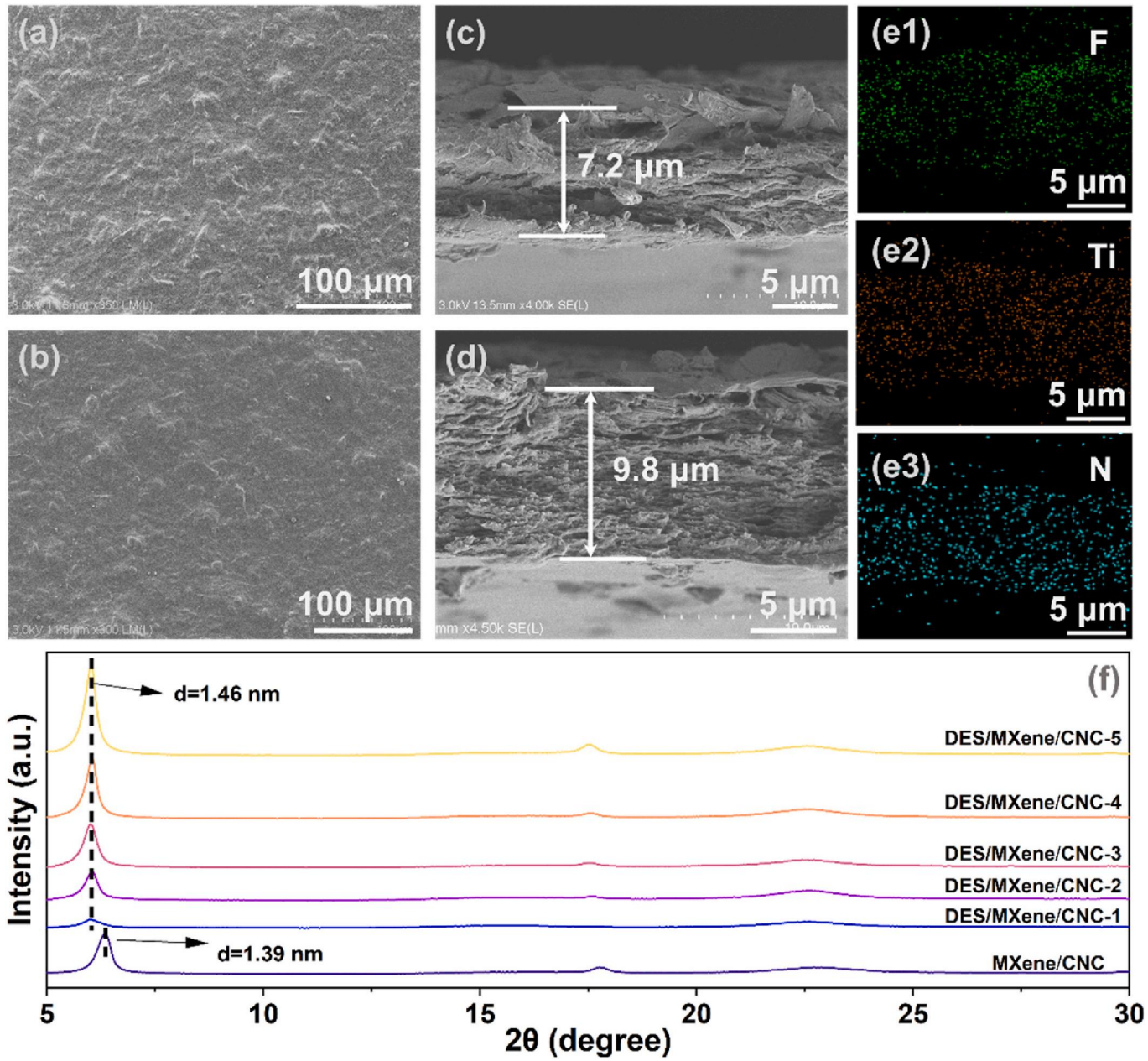

Fig. 4. SEM images of (a) the top surface and (c) cross-sectional surface of the MXene/CNC membrane. SEM images of (b) the top surface and (d) cross-sectional surface of the DES/MXene/CNC-4 membrane. (e) EDX mapping images of F, Ti, and N in the DES/MXene/CNC-4 cross-sectional image. (f) XRD patterns of MXene/CNC and DES/MXene/CNC membranes with different DES-I MXene contents.

continuous test was subsequently performed to evaluate the stability and durability of the DES/MXene/CNC-4 membrane (Fig. 5c). The composite membrane demonstrated excellent stability, maintaining consistent permeability and selectivity throughout the test. The practical application potential of the DES/MXene/CNC-4 membrane was further confirmed through mixed-gas separation experiments, where CO_2 permeability was slightly lower than that in single-gas tests. The separation factors for CO_2/N_2 and CO_2/CH_4 in the mixed-gas test were 81.7 and 91.8, respectively (detailed information in Table S1).

Fig. 5d and e compare the separation performance of the DES/MXene/CNC-4 membrane with that of other related composite membranes (detailed information in Table S2). The CO_2/CH_4 separation performance of the DES/MXene/CNC-4 membrane surpasses that of most state-of-the art membranes, exceeding both the 2008 Robeson upper bound [41] and the 2019 gas separation membrane upper bound [42]. The DES/MXene/CNC-4 membrane achieves superior performance because of its high CO_2 affinity, excellent interfacial compatibility, and suitable interlayer spacing of the MXene nanosheets.

A possible gas separation mechanism is proposed in Fig. 6. In membrane preparation, CO_2-philic DESs are used as intercalated agents and are confined to MXene nanochannels to regulate their interlayer spacing. The membrane follows solution diffusion and facilitated transport mechanisms. The solution-diffusion mechanism relies mainly on the interaction between the CNC matrix and CO_2, and the facilitated transport mechanism relies mainly on the interaction between the amine groups in DES and CO_2. The gas molecules encounter an energy barrier at the entrance of the MXene channel. The DES and terminal groups of MXenes form favorable interactions with CO_2 molecules, creating adsorption sites that preferentially pull CO_2 through channels *via* surface diffusion. N_2 and CH_4 molecules face a higher energy barrier to pass through the MXene channels. Moreover, an increase in the MXene interlayer spacing has a more significant effect on promoting CO_2

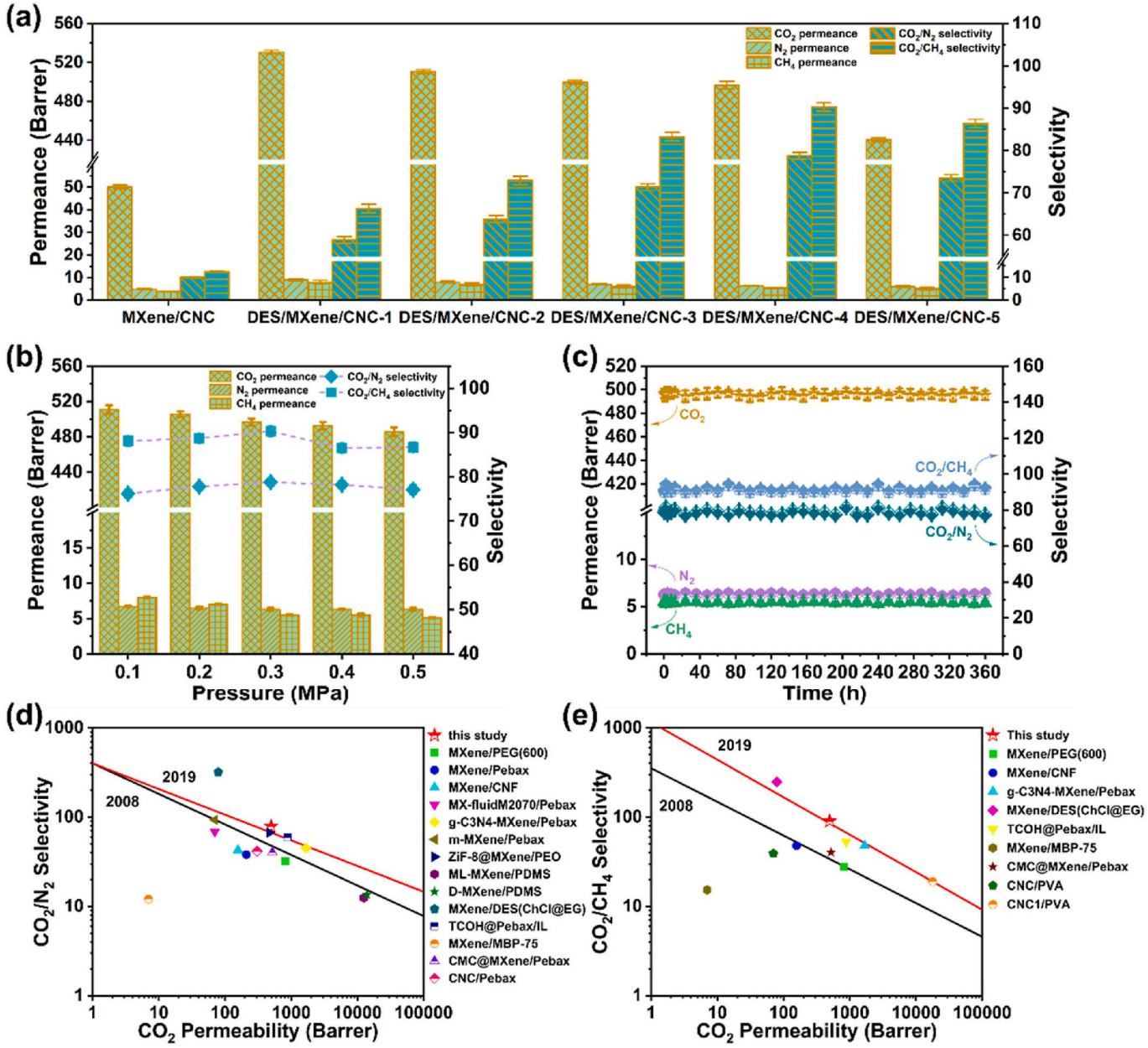

Fig. 5. (a) Single gas permeance and ideal selectivity over the MXene/CNC and DES/MXene/CNC membranes. Effects of DES/MXene/CNC-4 membranes with (b) different pressures and (c) 360-h long time test of gas separation performance. (d) CO_2/N_2 and (e) CO_2/CH_4 separation capability comparison of the DES/MXene/CNC-4 membrane with other composite membranes.

transfer than other gases do.

4. Conclusions

In this work, a DES/MXene/CNC composite membrane was fabricated. The interlayer spacing of MXenes is optimized by alkaline ChCl/urea DES and nanocellulose, leading to favorable CO_2 passage. The integration of MXene nanochannels with the unique solution-diffusion characteristics of cellulose and DES created a synergistic effect that jointly promoted CO_2 permeability and selectivity. The maximum CO_2 permeability of the composite membrane is 496.7 Barrer, and the ideal selectivities of CO_2/N_2 are 78.8 and 90.3, respectively, which are superior to those of most state-of-the-art CO_2 separation membranes. By leveraging the unique properties of MXenes and nanocellulose, combined with the tuning capabilities of DESs, this research opens new avenues for the design and fabrication of high-performance membranes tailored for carbon dioxide separation. This work contributes to the development of MXene and nanocellulose-based membranes for efficient carbon capture applications.

CRediT authorship contribution statement

Mengjie Li: Writing – original draft, Methodology, Formal analysis, Data curation. **Chuan Xu:** Writing – original draft, Methodology, Formal analysis, Data curation. **Miaomiao Wu:** Data curation. **Xiong-Fei Zhang:** Writing – original draft, Formal analysis, Conceptualization. **Jianfeng Yao:** Writing – review & editing, Supervision, Formal analysis, Conceptualization.

Declaration of competing interest

The authors declare that they have no known competing financial

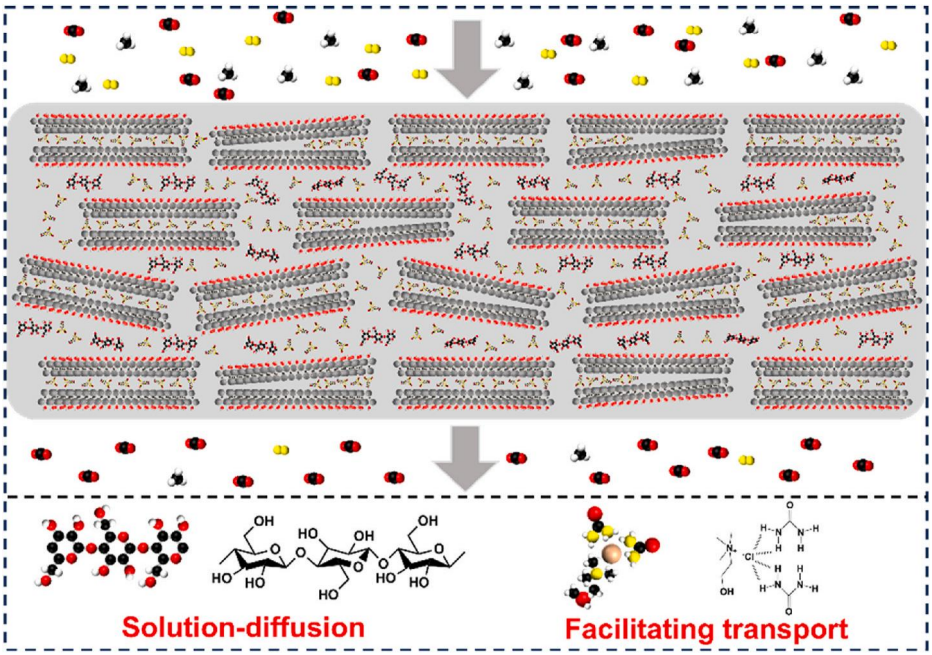

Fig. 6. Schematic diagram of the CO_2 separation mechanism of DES/MXene/CNC membranes.

interests or personal relationships that could have appeared to influence the work reported in this paper.

Acknowledgment

The authors are grateful for financial support from the National Natural Science Foundation of China (52103113) and the Forestry Science and Technology Innovation and Extension Project of Jiangsu Province (LYKJ [2021] 04).

Appendix A. Supplementary data

Supplementary data to this article can be found online at https://doi.org/10.1016/j.memsci.2025.124090.

Data availability

Data will be made available on request.

References

[1] Z. Zhou, T. Ma, H. Zhang, S. Chheda, H. Li, K. Wang, S. Ehrling, R. Giovine, C. Li, A. H. Alawadhi, M.M. Abduljawad, M.O. Alawad, L. Gagliardi, J. Sauer, O.M. Yaghi, Carbon dioxide capture from open air using covalent organic frameworks, Nature 635 (8040) (2024) 19–24, https://doi.org/10.1038/s41586-024-08080-x.

[2] C. Charalambous, E. Moubarak, J. Schilling, E. Sanchez Fernandez, J.-Y. Wang, L. Herraiz, F. McIlwaine, S.B. Peh, M. Garvin, K.M. Jablonka, S.M. Moosavi, J. Van Herck, A.Y. Ozturk, A. Pourghaderi, A.-Y. Song, G. Mouchaham, C. Serre, J. A. Reimer, A. Bardow, B. Smit, S. Garcia, A holistic platform for accelerating sorbent-based carbon capture, Nature 632 (8023) (2024) 89–94, https://doi.org/10.1038/s41586-024-07683-8.

[3] S.J. Datta, A. Mayoral, N.M.S. Bettahalli, P.M. Bhatt, M. Karunakaran, I.D. Carja, D. Fan, P.G.M. Mileo, R. Semino, G. Maurin, O. Terasaki, M. Eddaoudi, Rational design of mixed-matrix metal-organic framework membranes for molecular separations, Science 376 (6597) (2022) 1080, https://doi.org/10.1126/science.abe0192.

[4] G. Chen, C. Chen, Y. Guo, Z. Chu, Y. Pan, G. Liu, G. Liu, Y. Han, W. Jin, N. Xu, Solid-solvent processing of ultrathin, highly loaded mixed-matrix membrane for gas separation, Science 381 (6664) (2023) 1350–1356, https://doi.org/10.1126/science.adi1545.

[5] D. Zou, S.P. Nunes, I.F.J. Vankelecom, A. Figoli, Y.M. Lee, Recent advances in polymer membranes employing non-toxic solvents and materials, Green Chem. 23 (24) (2021) 9815–9843, https://doi.org/10.1039/d1gc03318b.

[6] S. Zhou, O. Shekhah, A. Ramírez, P. Lyu, E. Abou-Hamad, J. Jia, J. Li, P.M. Bhatt, Z. Huang, H. Jiang, T. Jin, G. Maurin, J. Gascon, M. Eddaoudi, Asymmetric pore windows in MOF membranes for natural gas valorization, Nature 606 (7915) (2022) 706–712, https://doi.org/10.1038/s41586-022-04763-5.

[7] L. Chen, G. Shi, J. Shen, B. Peng, B. Zhang, Y. Wang, F. Bian, J. Wang, D. Li, Z. Qian, G. Xu, G. Liu, J. Zeng, L. Zhang, Y. Yang, G. Zhou, M. Wu, W. Jin, J. Li, H. Fang, Ion sieving in graphene oxide membranes via cationic control of interlayer spacing, Nature 550 (7676) (2017) 380–383, https://doi.org/10.1038/nature24044.

[8] B. Zhu, S. He, Y. Yang, S. Li, C.H. Lau, S. Liu, L. Shao, Boosting membrane carbon capture via multifaceted polyphenol-mediated soldering, Nat. Commun. 14 (1) (2023), https://doi.org/10.1038/s41467-023-37479-9.

[9] Z. Li, Z. Li, N. Zhang, J. Bao, X. Zhang, G. He, C. Chen, Y. Song, Ultra-thin size-sieving gas separation membrane by precisely contra-diffusion-match growth of ZIF-67 among GO laminates, J. Membr. Sci. 694 (2024) 122428, https://doi.org/10.1016/j.memsci.2024.122428.

[10] H. Yang, M. Han, W. Zhang, M. Yi, L. Xia, F. Meng, Y. Wang, S. Zhao, High performance mixed-dimensional assembled MXene composite membranes for molecular sieving, J. Membr. Sci. 698 (2024) 122606, https://doi.org/10.1016/j.memsci.2024.122606.

[11] D. Xu, Y. Jin, C. Li, Y. Fan, S. Kawi, X. Meng, J. Song, N. Yang, COF/mXene composite membranes compact assembled by electrostatic interactions: a strategy for H_2/CO_2 separation, J. Membr. Sci. 700 (2024) 122678, https://doi.org/10.1016/j.memsci.2024.122678.

[12] Y. Kang, Y. Wang, H. Zhang, Z. Wang, X. Zhang, H. Wang, Functionalized 2D membranes for separations at the 1-nm scale, Chem. Soc. Rev. 53 (15) (2024) 7939–7959, https://doi.org/10.1039/d4cs00272e.

[13] D.I. Petukhov, A.S. Kan, A.P. Chumakov, O.V. Konovalov, R.G. Valeev, A. A. Eliseev, MXene-based gas separation membranes with sorption type selectivity, J. Membr. Sci. 621 (2021) 118994, https://doi.org/10.1016/j.memsci.2020.118994.

[14] X. Qiu, Y. Zheng, H. Li, K. Qu, H. Yan, R. Li, Unveiling gas transport mechanisms in tunable MXene nanochannels: insights from molecular dynamics simulations, J. Membr. Sci. 715 (2025) 123459, https://doi.org/10.1016/j.memsci.2024.123459.

[15] M. Rezakazemi, A.A. Shamsabadi, H. Lin, P. Luis, S. Ramakrishna, T. M. Aminabhavi, Sustainable MXenes-based membranes for highly energy-efficient separations, Renew. Sustain. Energy Rev. 143 (2021) 110878, https://doi.org/10.1016/j.rser.2021.110878.

[16] Z. Shi, S. Liao, Y. Wei, L. Li, Theoretical insights into He/CH_4 separation by MXene nanopore, Chem. Eng. Sci. 287 (2024) 119781, https://doi.org/10.1016/j.ces.2024.119781.

[17] H. Lin, K. Gong, P. Hykys, D. Chen, W. Ying, Z. Sofer, Y. Yan, Z. Li, X. Peng, Nanoconfined deep eutectic solvent in laminated MXene for efficient CO_2 separation, Chem. Eng. J. 405 (2021) 126961, https://doi.org/10.1016/j.cej.2020.126961.

[18] B. Nowosielski, D. Warmińska, I. Cichowska-Kopczyńska, CO2 separation using supported deep eutectic liquid membranes based on 1,2-propanediol, ACS Sustain. Chem. Eng. 11 (10) (2023) 4093–4105, https://doi.org/10.1021/acssuschemeng.2c06278.

[19] M. Xu, H. Dou, Y. Ren, F. Peng, X. Xiao, X. Tantai, Y. Sun, B. Jiang, N. Yang, L. Zhang, Deep eutectic solvent membranes designed by the same-anion strategy for highly efficient ethylene/ethane separation, ACS Sustain. Chem. Eng. 10 (12) (2022) 4002–4012, https://doi.org/10.1021/acssuschemeng.2c00253.

[20] L. Ding, Y. Wei, L. Li, T. Zhang, H. Wang, J. Xue, L.-X. Ding, S. Wang, J. Caro, Y. Gogotsi, MXene molecular sieving membranes for highly efficient gas separation, Nat. Commun. 9 (1) (2018), https://doi.org/10.1038/s41467-017-02529-6.
[21] K. Wang, D. Chen, J. Tang, Z. Hong, Z. Zhu, Z. Yuan, Z. Lin, Y. Liu, R. Semiat, X. He, PIM-1-based membranes mediated with CO_2-philic MXene nanosheets for superior CO_2/N_2 separation, Chem. Eng. J. 483 (2024) 149305, https://doi.org/10.1016/j.cej.2024.149305.
[22] M. Yahia, D. Refaat, J. Coronas, C. Tellez, Enhancing CO_2/CH_4 separation performance in PIM-1 based MXene nanosheets mixed matrix membranes, Sep. Purif. Technol. 356 (2025) 129825, https://doi.org/10.1016/j.seppur.2024.129825.
[23] M. Jia, X.-F. Zhang, Y. Feng, Y. Zhou, J. Yao, In-situ growing ZIF-8 on cellulose nanofibers to form gas separation membrane for CO_2 separation, J. Membr. Sci. 595 (2020) 117579, https://doi.org/10.1016/j.memsci.2019.117579.
[24] C. Xu, X.-F. Zhang, Z. Wang, J. Yao, Nanocellulose membrane with double-salt deep eutectic solvent for efficient carbon capture, Sep. Purif. Technol. 347 (2024) 127614, https://doi.org/10.1016/j.seppur.2024.127614.
[25] Z. Hu, H. Zhang, X.-F. Zhang, M. Jia, J. Yao, Polyethylenimine grafted ZIF-8@cellulose acetate membrane for enhanced gas separation, J. Membr. Sci. 662 (2022) 120996, https://doi.org/10.1016/j.memsci.2022.120996.
[26] S. Foorginezhad, X. Ji, Developing slurry based on immobilized and aqueous [MEACl][EDA] for CO_2 capture, Chem. Eng. J. 499 (2024) 156176, https://doi.org/10.1016/j.cej.2024.156176.
[27] W. Zhang, X.-X. Ji, M.-G. Ma, Emerging MXene/cellulose composites: design strategies and diverse applications, Chem. Eng. J. 458 (2023) 141402, https://doi.org/10.1016/j.cej.2023.141402.
[28] Y. Wang, M. Ding, W. Rong, S. Kong, J. Yao, In situ growth of Fe-doped zeolitic imidazolate framework on MXene for boosting photodriven CO_2 cycloaddition, Sep. Purif. Technol. 345 (2024) 127399, https://doi.org/10.1016/j.seppur.2024.127399.
[29] J. Wu, Y. Wang, Y. Zhang, H. Meng, Y. Xu, Y. Han, Z. Wang, Y. Dong, X. Zhang, Highly safe and ionothermal synthesis of Ti_3C_2 MXene with expanded interlayer spacing for enhanced lithium storage, J. Energy Chem. 47 (2020) 203–209, https://doi.org/10.1016/j.jechem.2019.11.029.
[30] Y. Jia, F. Shi, H. Li, Z. Yan, J. Xu, J. Gao, X. Wu, Y. Li, J. Wang, B. Zhang, Facile ionization of the nanochannels of lamellar membranes for stable ionic liquid immobilization and efficient CO_2 separation, ACS Nano 16 (9) (2022) 14379–14389, https://doi.org/10.1021/acsnano.2c04670.
[31] J. Kim, Y. Yoon, S.K. Kim, S. Park, W. Song, S. Myung, H.K. Jung, S.S. Lee, D. H. Yoon, K.S. An, Chemically stabilized and functionalized 2D-MXene with deep eutectic solvents as versatile dispersion medium, Adv. Funct. Mater. 31 (13) (2021) 202008722, https://doi.org/10.1002/adfm.202008722.
[32] Q. Shan, Q. Ding, W. Wu, Preparation of antioxidative MXene by deep eutectic solvent-assisted electrochemical ultrasonic composite exfoliation and its application in flexible solid-state supercapacitors, Ind. Eng. Chem. Res. 62 (24) (2023) 9492–9502, https://doi.org/10.1021/acs.iecr.3c00989.
[33] S. Wang, X. Peng, L. Zhong, S. Jing, X. Cao, F. Lu, R. Sun, Choline chloride/urea as an effective plasticizer for production of cellulose films, Carbohydr. Polym. 117 (2015) 133–139, https://doi.org/10.1016/j.carbpol.2014.08.113.
[34] B. Jiang, H. Dou, L. Zhang, B. Wang, Y. Sun, H. Yang, Z. Huang, H. Bi, Novel supported liquid membranes based on deep eutectic solvents for olefin-paraffin separation via facilitated transport, J. Membr. Sci. 536 (2017) 123–132, https://doi.org/10.1016/j.memsci.2017.05.004.
[35] Z. Wang, M. Li, X.-F. Zhang, Y. Zhou, J. Yao, Integration of natural clay into cellulose membrane for efficient CO_2/N_2 separation, Cellulose 29 (3) (2022) 1873–1881, https://doi.org/10.1007/s10570-021-04407-3.
[36] Q. Chen, Y. Chen, C. Wu, Probing the evolutionary mechanism of the hydrogen bond network of cellulose nanofibrils using three DESs, Int. J. Biol. Macromol. 234 (2023) 123694, https://doi.org/10.1016/j.ijbiomac.2023.123694.
[37] Z. Wei, D. Wang, Y. Chen, D. Yu, Q. Ding, R. Li, C. Wu, The H-bond evolution of cellulose nanofibrils treated with choline chloride/oxalic acid, Cellulose 29 (7) (2022) 3675–3687, https://doi.org/10.1007/s10570-022-04517-6.
[38] C. Cai, L. Zhang, X. Meng, B. Luo, Y. Liu, M. Chi, J. Wang, T. Liu, S. Zhang, S. Wang, S. Nie, Mechanically robust triboelectric aerogels enabled by dense bridging of MXene, Nano Lett. 24 (50) (2024) 16022–16030, https://doi.org/10.1021/acs.nanolett.4c04401.
[39] Z. Hu, Y. Yang, X.-F. Zhang, C. Xu, J. Yao, Integrating two-dimensional MXene fillers into nanocellulose for the fabrication of CO_2 separation membranes, Sep. Purif. Technol. 326 (2023) 124704, https://doi.org/10.1016/j.seppur.2023.124704.
[40] M. Ishaq, M.A. Gilani, F. Ahmad, Z.M. Afzal, I. Arshad, M.R. Bilad, K. Ayub, A. L. Khan, Theoretical and experimental investigation of CO_2 capture through choline chloride based supported deep eutectic liquid membranes, J. Mol. Liq. 335 (2021) 116234, https://doi.org/10.1016/j.molliq.2021.116234.
[41] L.M. Robeson, The upper bound revisited, J. Membr. Sci. 320 (1–2) (2008) 390–400, https://doi.org/10.1016/j.memsci.2008.04.030.
[42] B. Comesaña-Gándara, J. Chen, C.G. Bezzu, M. Carta, I. Rose, M.-C. Ferrari, E. Esposito, A. Fuoco, J.C. Jansen, N.B. McKeown, Redefining the Robeson upper bounds for CO_2/CH_4 and CO_2/N_2 separations using a series of ultrapermeable benzotriptycene-based polymers of intrinsic microporosity, Energy Environ. Sci. 12 (9) (2019) 2733–2740, https://doi.org/10.1039/c9ee01384a.